



The role of “ZrF₄-modification” on the structure and electrochemical performance of Li₄Ti₅O₁₂ anode material

Wen Li ^{a, b}, Xue Bai ^{a, b}, Lihui Zhang ^{a, b, *}, Aijia Wei ^{a, b}, Xiaohui Li ^{a, b}, Zhenfa Liu ^{a, b, **}

^a Institute of Energy Resources, Hebei Academy of Sciences, Shijiazhuang, Hebei Province 050081, PR China

^b Hebei Engineer Research Center for Water Saving in Industry, Shijiazhuang, Hebei Province 050081, PR China

ARTICLE INFO

Article history:

Received 20 October 2017

Received in revised form

31 January 2018

Accepted 15 February 2018

Available online 16 February 2018

Keywords:

Li₄Ti₅O₁₂

ZrF₄

Modification

Lithium ion batteries

ABSTRACT

In order to determine the reaction mechanism of the fluoride modification process and its influence on the electrochemical properties of Li₄Ti₅O₁₂ anode material, the “ZrF₄-modified” Li₄Ti₅O₁₂ was prepared via a co-precipitation method. Structural characterization results shows that both Zr⁴⁺ and F⁻ ions were not incorporated into the lattice structure of Li₄Ti₅O₁₂ after the modification process. Instead, F⁻ reacts with Li₄Ti₅O₁₂ chemically to generate new impurity phase such as anatase TiO₂ and LiF, while Zr⁴⁺ forms amorphous ZrO₂ nano-particles over the Li₄Ti₅O₁₂ particles. There was no dense coating layer formed on the surface of the Li₄Ti₅O₁₂ particles. These results indicate the reaction mechanism of the ZrF₄-modification process was different from that previously reported (such as “AlF₃, MgF₂, ZnF₂, SrF₂ and CaF₂-modification”). The rate capability and cycling stability of Li₄Ti₅O₁₂ can be enhanced due to the “ZrF₄-modification” process. Specifically, the 2 wt% “ZrF₄-modified” Li₄Ti₅O₁₂ shows the best electrochemical performance.

© 2018 Elsevier B.V. All rights reserved.

1. Introduction

Surface modification, especially with fluorides has been developed to improve the electrochemical performance of electrode materials for lithium ion batteries (LIBs) [1–16]. Recently, AlF₃ [1–9], CaF₂ [10,11], SrF₂ [12,13], LiF [14], LaF₃ [15] and ZrF_x [16] have been widely used to modify cathode materials for improving their electrochemical performance. The modification process involves generation of a fluoride precipitate with a metal nitrate and ammonium fluoride, and then chemical co-precipitation followed by low-temperature calcination, which leads to the formation of a fluoride coating layer over an electrode surface. The enhanced performance was attributed to the fact that the fluoride coating material which exhibits thermal stability and an inert behavior with hydrofluoric acid, could prevent the electrode material from reacting with hydrofluoric acid and effectively enhance its cycling stability [1–16].

Additionally, AlF₃ has been first used to modify the Li₄Ti₅O₁₂

anode material [17], showing that instead of the formation of an AlF₃ coating layer, Al³⁺ and F⁻ ions were incorporated into the Li₄Ti₅O₁₂ lattice structure with the production of a small amount of anatase TiO₂ after the modification process. The modified Li₄Ti₅O₁₂ anodes delivered slightly higher discharge capacity and exhibited excellent long-term cycling stability compared to the pure Li₄Ti₅O₁₂. The improved electrochemical performance could be attributed to the facts that [17]: (1) co-doping of Al³⁺ and F⁻ could improve both ionic and electronic conductivities of the Li₄Ti₅O₁₂; (2) the *in situ* generated TiO₂ could enhance the ionic diffusion in the electrode by restraining the growth of Li₄Ti₅O₁₂ particles and by providing a short ionic diffusion path through the boundary among TiO₂ and Li₄Ti₅O₁₂; and (3) the F⁻ doping could prevent the Li₄Ti₅O₁₂ particles from the attack by acidic species present in the electrolyte, such as hydrofluoric acid. Our previous work showed that AlF₃-modification can usefully restrain the gas-release problem of LIBs using Li₄Ti₅O₁₂ as the anode material [18]. The results indicated that electrolyte reduction decomposition was suppressed by the coating layer formed on the surface of Li₄Ti₅O₁₂ after the AlF₃ modification process, thereby preventing the gas generation during cycling tests. To further understand the reaction mechanism of the fluoride modification process, MgF₂ [19] and ZnF₂ [20] were both used to separately modify Li₄Ti₅O₁₂, respectively. The results show that F⁻ reacted with Li₄Ti₅O₁₂ to produce a new impurity phase

* Corresponding author. Institute of Energy Resources, Hebei Academy of Sciences, Shijiazhuang, Hebei Province 050081, PR China.

** Corresponding author. Institute of Energy Resources, Hebei Academy of Sciences, Shijiazhuang, Hebei Province 050081, PR China.

E-mail addresses: zlhkxy@126.com (L. Zhang), liuzhenfa@hebut.edu.cn (Z. Liu).

composed of anatase TiO₂ and LiF, while the Mg²⁺ ions and Zn²⁺ produced the MgO and ZnO coating layers on the surface of Li₄Ti₅O₁₂ particles, respectively [30,31]. The above mentioned MgO and ZnO coating layers effectively curbed the electrolyte reduction decomposition, thereby improving the electrochemical properties. Li et al. [21] chose SrF₂ to modify Li₄Ti₅O₁₂, and indicated that Sr²⁺ and F⁻ could not incorporate into the bulk phase of the Li₄Ti₅O₁₂, but instead formed a SrF₂ coating layer on the surface of the Li₄Ti₅O₁₂, which covered the catalytic active sites of the Li₄Ti₅O₁₂ and suppressed the electrolyte reduction decomposition on the surface of the Li₄Ti₅O₁₂, thus improving the electrochemical performance. Recently, we used CaF₂ to modify commercial Li₄Ti₅O₁₂, and found that F⁻ ions reacted with Ca²⁺ ions to form microscale CaF₂ crystals stacked on the surface of Li₄Ti₅O₁₂ particles instead of a CaF₂ coating layer which not only reduced the electrode polarization, but also partially suppressed the reductive decomposition, both of which were beneficial to the promotion of the electrochemical performance of Li₄Ti₅O₁₂ [22].

Summarily, the reaction mechanism of the fluoride modification process for Li₄Ti₅O₁₂ highly depends on the composition of the coating materials. So far, ZrF₄ has not been used to modify Li₄Ti₅O₁₂ anode material and the reaction mechanism of the ZrF₄-modification process is not clearly known. In this paper, the “ZrF₄-modified” Li₄Ti₅O₁₂ was obtained via the above-mentioned co-precipitation method for the first time to our knowledge, and the reaction mechanism of the ZrF₄-modification process is further investigated systematically.

2. Experimental

Li₄Ti₅O₁₂ materials used in this work were obtained from Sichuan Xingneng New Materials Co. For those coated materials, Li₄Ti₅O₁₂ powder was first dispersed in the deionized water. Next, ammonium fluoride (NH₄F, AR) and magnaliumnitrate non-hydrate [Zr(NO₃)₄·5H₂O, AR] were added into the above obtained Li₄Ti₅O₁₂ suspension based on the fixed stoichiometric molar ratio of Zr⁴⁺/F⁻ = ¼, and various coating amounts were chosen. The Li₄Ti₅O₁₂ powder in the suspension was then collected and dried at 80 °C for 10 h. Finally, the ZrF₄-modified Li₄Ti₅O₁₂ samples used in this work were obtained by calcining the above drying powder at 400 °C for 5 h under argon atmosphere. All ZrF₄-modified Li₄Ti₅O₁₂ samples were designated *m*ZFLTO, where *m* denotes the weight ratio of ZrF₄/Li₄Ti₅O₁₂ (i.e. *m* = 1, 2, and 3). The Li₄Ti₅O₁₂ was also modified with Zr⁴⁺ and F⁻, denoted 2MLTO and 2FLTO, respectively.

Powder XRD patterns were collected over a 2θ range of 10°–90° to identify the phase composition and crystal lattice parameters of all the Li₄Ti₅O₁₂ samples using CuKα X-rays (1.5406 Å at 40 kV and 40 mA) on an Ultima IV (Rigaku) X-ray diffractometer. The particulate morphology and the coating layer of the Li₄Ti₅O₁₂ samples using a scanning electron microscope (SEM, Sirion 200 FEI Netherlands) and a transmission electron microscope (TEM, JEOL JEM-2100plus). Chemical composition of the coating layer for the modified- Li₄Ti₅O₁₂ samples were determined by X-ray photoelectron spectroscopy (XPS, PHI5600 Physical Electronics).

Electrochemical characterization of the Li₄Ti₅O₁₂ samples were performed by assembling 2032 coin-cells, which were consist of a Li₄Ti₅O₁₂ electrode disc and a piece of lithium metal separated by a polymer separator. The Li₄Ti₅O₁₂ electrode used in this work was made by mixing 85 wt% as-prepared samples (pure Li₄Ti₅O₁₂ and the modified Li₄Ti₅O₁₂ samples) with 10 wt% conductive carbon (Super-P) and 5 wt% polyvinylidene fluoride binder using N-methyl pyrrolidone as a solvent to form a slurry. Then, the obtained slurry was coated on a Cu foil by painting. Afterward, the working electrode was dried in a vacuum oven at 105 °C for 12 h to remove any residual solvent and the adsorbed moisture. The coin-cell was

assembled in an argon-filled glove box using the as-prepared Li₄Ti₅O₁₂ as working electrode, 1 mol L⁻¹ solution of LiPF₆ in ethylene carbonate, dimethyl carbonate, and diethyl carbonate (volume ratio 1:1:1) (Capchem Technology (Shenzhen) Co., Ltd.) as the electrolyte, a microporous polypropylene membrane (Celgard 2400, Celgard Inc., USA) as a separator and lithium foil as a counter electrode.

Galvanostatic charge and discharge experiments were carried out on an automatic galvanostatic (dis)charge unit (Land CT 2001A, Wuhan, China) between 0 and 3 V at different rates at 25 °C. The coin-type half cells were firstly (dis)charged at different C-rates (0.5, 1, 3, 5, 10 C and 0.5 C) for five cycles, and then discharged and charged at a 5-C ate for another 195 times. Cyclic voltammetry (CV) and electrochemical impedance spectroscopy (EIS) tests were conducted on an electrochemical workstation (Interface 3000, Gamry, USA). For the CV measurements, the potential range was set from 0 to 3 V while the scan rate was set at 0.2 mV s⁻¹. The EIS measurements were performed in the frequency range of 10 mHz–100 kHz before discharge-charge tests for the first time, at first charging up to 1.6 V for the second time and at 21st charging up to 1.6 V for the third time with a current density of 1 C rate in the voltage range of 0–3 V, respectively.

3. Results and discussion

XRD patterns of all samples are shown in Fig. 1(a)–(c) and the standard XRD patterns of Si, rutile TiO₂, anatase TiO₂, LiF and Li₄Ti₅O₁₂ are shown in Fig. 1d. Internal standard and calibration curves are used to analyze the lattice parameters of all materials, and the diffraction peaks of standard Si are marked with asterisks (*). Among all investigated samples, the major diffraction peaks were in accordance with the standard patterns of Li₄Ti₅O₁₂ with PDF number of 72–0426, suggests that the modification process does not change the basic Li₄Ti₅O₁₂ structure. The lattice parameters of all samples (shown in Table 1) were obtained by the Rietveld refinement and the obtained lattice constants for all those samples are 8.3568(5), 8.3568(6), 8.3568(8), 8.3569(3), 8.3568(7), and 8.3569(4) for pure Li₄Ti₅O₁₂, 1ZFLTO, 2ZFLTO, 3ZFLTO, 2FLTO and 2LTO, respectively. Previous research showed that the substitution of Ti⁴⁺ with Zr⁴⁺ ions for Li₄Ti₅O₁₂ increases the lattice parameter due to the larger ionic radius of Zr⁴⁺ (0.072 nm) compared to Ti⁴⁺ (0.0605 nm) [23–25]. Moreover, the introduction of Zr⁴⁺ ions in Li₄Ti₅O₁₂ can form the anatase TiO₂. However, in our case, no lattice parameter changes and anatase TiO₂ were detected for 2ZLTO sample, suggesting that Zr⁴⁺ ions do not incorporate the Li₄Ti₅O₁₂ lattice after the modification process. After the introduction of F⁻ into the Li₄Ti₅O₁₂ particles, F⁻ will incorporate the [O]^{32e} site, causing the transition of a certain amount of Ti ions from Ti⁴⁺ to Ti³⁺ due to the charge compensation [26]. It is well known that the incorporation of F⁻ into the Li₄Ti₅O₁₂ lattice causes the decrease of the lattice parameter, based on Vegard's law. Although the smaller radius of F⁻ ions (0.133 nm) compared to that of O²⁻ (0.140 nm) will cause the shrinkage of the lattice, while the radius of Ti³⁺ (0.067 nm) being larger than that of Ti⁴⁺ (0.0605 nm) will expand the lattice, the former plays a leading role in determining the lattice parameter and thus leads a decrease of the lattice constants due to the incorporation of F into the structure [27]. The lattice parameter of 2FLTO has almost the same value as that for the pure Li₄Ti₅O₁₂, indicating that no F⁻ ions incorporate into the Li₄Ti₅O₁₂ structure after the modification process. Additionally, the lattice parameters of *m*ZFLTO samples are quite similar to that of the pure Li₄Ti₅O₁₂, showing that both Zr⁴⁺ and F⁻ are not incorporated into the Li₄Ti₅O₁₂ lattice after the modification process. Moreover, 2FLTO shows extra peaks indexed to anatase TiO₂ and LiF due to the fact that F⁻ has chemically reacted with Li₄Ti₅O₁₂ [19]. Interestingly,

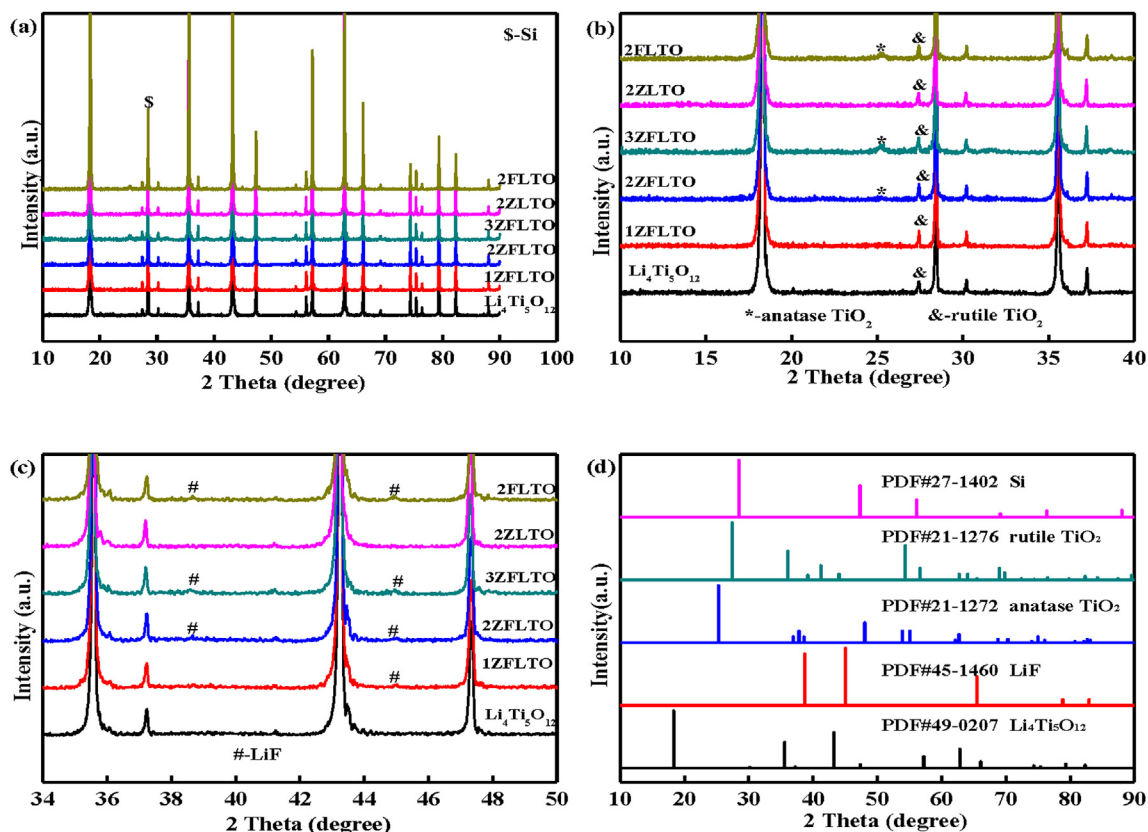


Fig. 1. XRD patterns of all samples in the range of (a) 10–90°, (b) 10–40°, (c) 34–50°, (d) standard XRD patterns of Si, rutile TiO₂, anatase TiO₂, LiF and Li₄Ti₅O₁₂.

Table 1

Lattice parameters of all samples.

Samples	Lattice parameters		Interplanar spacing d/Å
	$a/\text{Å}$	$V/\text{Å}^3$	
Li ₄ Ti ₅ O ₁₂	8.35685	583.61685	4.82483
1ZFLTO	8.35686	583.61894	4.82484
2ZFLTO	8.35688	583.62313	4.82485
3ZFLTO	8.35693	583.63361	4.82487
2FLTO	8.35687	583.62104	4.82484
2ZLTO	8.35694	583.63570	4.82488

these *m*ZFLTO samples also exhibit diffraction peaks due to anatase and LiF, and the intensity of which increases with both the increasing of *m* value and the introduction of F⁻ amount. Summarily, Zr⁴⁺ is chemically stable with Li₄Ti₅O₁₂ while F⁻ is chemically unstable with Li₄Ti₅O₁₂ during the “ZrF₄-modification” process. It is noteworthy that no diffraction peaks indexed to ZrF₄ were observed for all of the *m*ZFLTO samples, providing that no ZrF₄ was formed during the modification process.

Fig. 2 displays the SEM images of pure Li₄Ti₅O₁₂ and modified Li₄Ti₅O₁₂ samples. The pure Li₄Ti₅O₁₂ particles show a well-crystallized structure and a smooth surface. In contrast, the 2ZFLTO, 2FLTO, and 2ZLTO particles present a rough surface and there are some tiny particles on the surface of the Li₄Ti₅O₁₂ particles, which might be the generated impurity phase. The tiny particles on the 2FLTO particles should be generated anatase TiO₂ and LiF during the modification process [19]. XPS measurements were performed to clarify the generated impurity phases on the 2ZFLTO particles and the corresponding results are shown in Fig. 3. Not only were Ti, O, and Li elements detected by XPS, but Zr and F elements

were also found. The Ti 2p spectrum of the 2ZFLTO sample in Fig. 3a consists of a Ti 2p_{3/2} peak at 458.32 eV and a Ti 2p_{1/2} peak at 463.98 eV, which can be assigned to Ti⁴⁺. Moreover, the peak at 529.87 eV in the O 1s spectrum shown in Fig. 3c also proves the presence of O²⁻. The combination of Ti and O spectra prove the formation of TiO₂. The peaks observed at 685.15 eV in the F 1s spectrum shown in Fig. 3d and 50.32 eV in the Li 1s spectrum shown in Fig. 3f are both related to LiF. These XPS results further demonstrate that TiO₂ and LiF exist on the 2MFLTO particles, which is in good agreement with the XRD results. The pair of Zr 3d_{3/2} peaks located at 182.15 and 184.49 eV appear in the Zr 3d spectrum shown in Fig. 3e are in good agreement with ZrO₂. The peak at 531.58 eV in the O 1s XPS spectrum in Fig. 3c also certifies the presence of O²⁻. Therefore, the Zr⁴⁺ ions form ZrO₂ instead of ZrF₄ after the modification process. Previous XRD results show that no diffraction peaks belonging to ZrO₂ were detected; that is, the ZrO₂ impurity clarified here is most likely to exist on the Li₄Ti₅O₁₂ particles as an amorphous state. In order to clarify the existence of amorphous ZrO₂ on the surface of Li₄Ti₅O₁₂ particles, high-

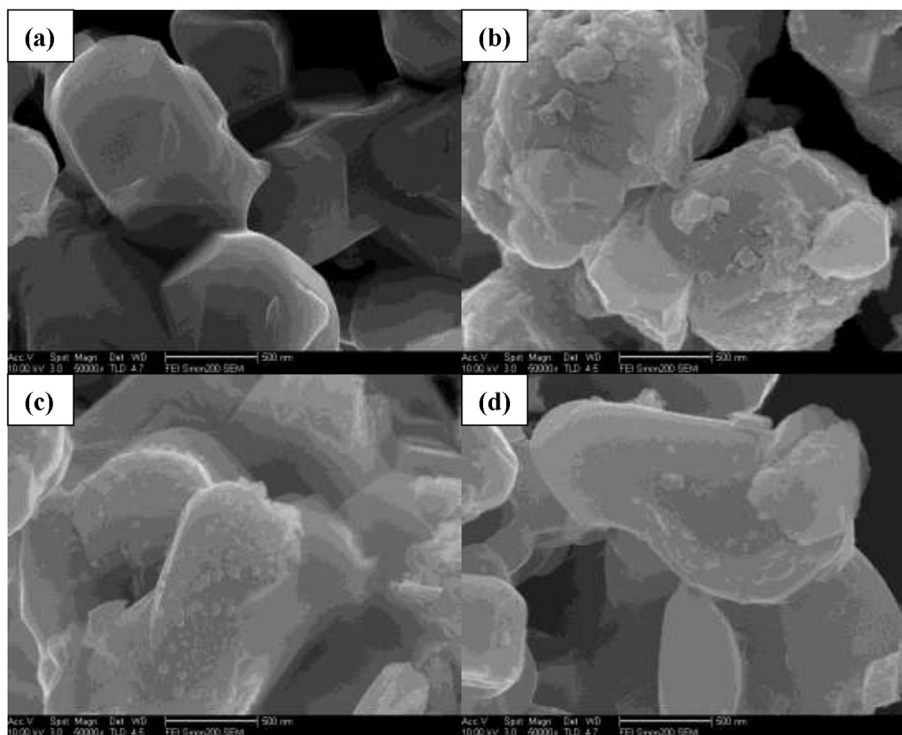


Fig. 2. SEM images of (a) pure $\text{Li}_4\text{Ti}_5\text{O}_{12}$, (b) 2ZFLTO, (c) 2FLTO and (d) 2ZLTO sample.

resolution TEM (HRTEM) was carried out in 2ZFLTO and 2ZLTO samples. As shown in Fig. 4, the 2ZFLTO and 2ZLTO particles are covered with nano-particles showing no crystal plane but an amorphous state, which is consistent with previous XRD results. Moreover, instead of being homogeneously distributed, these nano-particles are isolatedly distributed on the surface of $\text{Li}_4\text{Ti}_5\text{O}_{12}$ particles. No dense ZrO_2 coating layer was detected on the surface of the 2ZFLTO and 2ZLTO particles.

In order to study the effects of the ZrF_4 -modification process, the electrochemical properties of the pure $\text{Li}_4\text{Ti}_5\text{O}_{12}$ and modified $\text{Li}_4\text{Ti}_5\text{O}_{12}$ samples were tested systematically. Fig. 5a shows the CV curves of the pure $\text{Li}_4\text{Ti}_5\text{O}_{12}$, mZFLTO and 2ZLTO samples in the range of 0–3 V at 0.2 mV s^{-1} . As shown in Fig. 5a, the cathodic and anodic peaks at respective approximately 1.7 and 1.5 V, respectively, are attributed to the redox of $\text{Ti}^{4+}/\text{Ti}^{3+}$, and the reduction and oxidation peaks below 0.6 V are caused by a multi-step restoration of Ti^{4+} [17–22]. It is worth noting that there is an obvious irreversible peak appearing at approximately 0.7 V during the reduction process for all samples, which is due to the electrolyte reduction decomposition on the $\text{Li}_4\text{Ti}_5\text{O}_{12}$ particles. It has been proved that the irreversible peak disappears completely at approximately 0.7 V for the MgF_2 - or ZnF_2 -modified $\text{Li}_4\text{Ti}_5\text{O}_{12}$ samples, due to the amorphous MgO or ZnO coating layer formed during the modification process which could suppress the electrolyte reduction decomposition on the $\text{Li}_4\text{Ti}_5\text{O}_{12}$ particles detected in our previous study. It also demonstrates that the irreversible peak at approximately 0.7 V of the CaF_2 -modified LTO sample partly disappears, which is attributed to the fact that the stacked CaF_2 crystals formed during the modification process could cover part of the active sites on the surface of the $\text{Li}_4\text{Ti}_5\text{O}_{12}$ particles thereby restraining the electrolyte reduction decomposition. However, the irreversible peaks at approximately 0.7 V for the mZFLTO and 2ZLTO samples almost does not disappear, suggesting that the electrolyte reduction decomposition could not be suppressed effectively. This could be ascribed to the fact that there is no dense coating layer

formed on the surface of $\text{Li}_4\text{Ti}_5\text{O}_{12}$ particles, and that the ZrO_2 nano-particles on the $\text{Li}_4\text{Ti}_5\text{O}_{12}$ could not cover all of the active sites on the surface of the $\text{Li}_4\text{Ti}_5\text{O}_{12}$ particles. It is noteworthy that the peak intensity for the electrolyte reduction decomposition of 2ZFLTO becomes obviously weaker than that of pure $\text{Li}_4\text{Ti}_5\text{O}_{12}$, indicating that the electrolyte reduction decomposition is restrained partially due to the ZrO_2 nano-particles formed on the $\text{Li}_4\text{Ti}_5\text{O}_{12}$. Moreover, the mZFLTO samples also show an extra pair of redox peaks in the range of 1.6–2.1 V and the current response of this redox reaction increases with increasing modification content, which is ascribed to the Li^+ insertion into and de-insertion out of anatase TiO_2 [17–19]. However, the 2ZLTO samples exhibit no extra pair of redox peaks in the range of 1.6–2.1 V due to the fact that no anatase TiO_2 formed during the modification process. The CV test results further testify to the fact that F^- will react with $\text{Li}_4\text{Ti}_5\text{O}_{12}$ first to form anatase TiO_2 for the mZFLTO samples. Fig. 5b exhibits the galvanostatic charge-discharge curves of pure LTO, mZFLTO and 2ZLTO samples at a 0.5 C-rate in the range of 0–3 V. The galvanostatic charge-discharge curves of all samples demonstrate a long range of flat voltage at approximately 1.5 V during the discharge process and at approximately 1.6 V during charge process, which are assigned to the Li^+ insertion and de-insertion of two-phase reaction and are also correspond to the one pair of strong redox peaks in the CV curves shown in Fig. 5. Moreover, the galvanostatic charge-discharge curves of all samples exhibit a short range of flat voltage at approximately 0.7 V during the discharge process due to the electrolyte reduction decomposition, suggesting that the electrolyte reduction decomposition could not be suppressed effectively after the modification process. It is worth noting that 2ZFLTO presents a range of flat voltage at approximately 0.7 V that is shorter than that of pure LTO, further proving that the electrolyte reduction is partially suppressed. Thus, both the results from the CV curves and galvanostatic charge-discharge curves illustrate that the electrolyte reduction decomposition could not be suppressed effectively, due to the fact that there is no dense coating layer

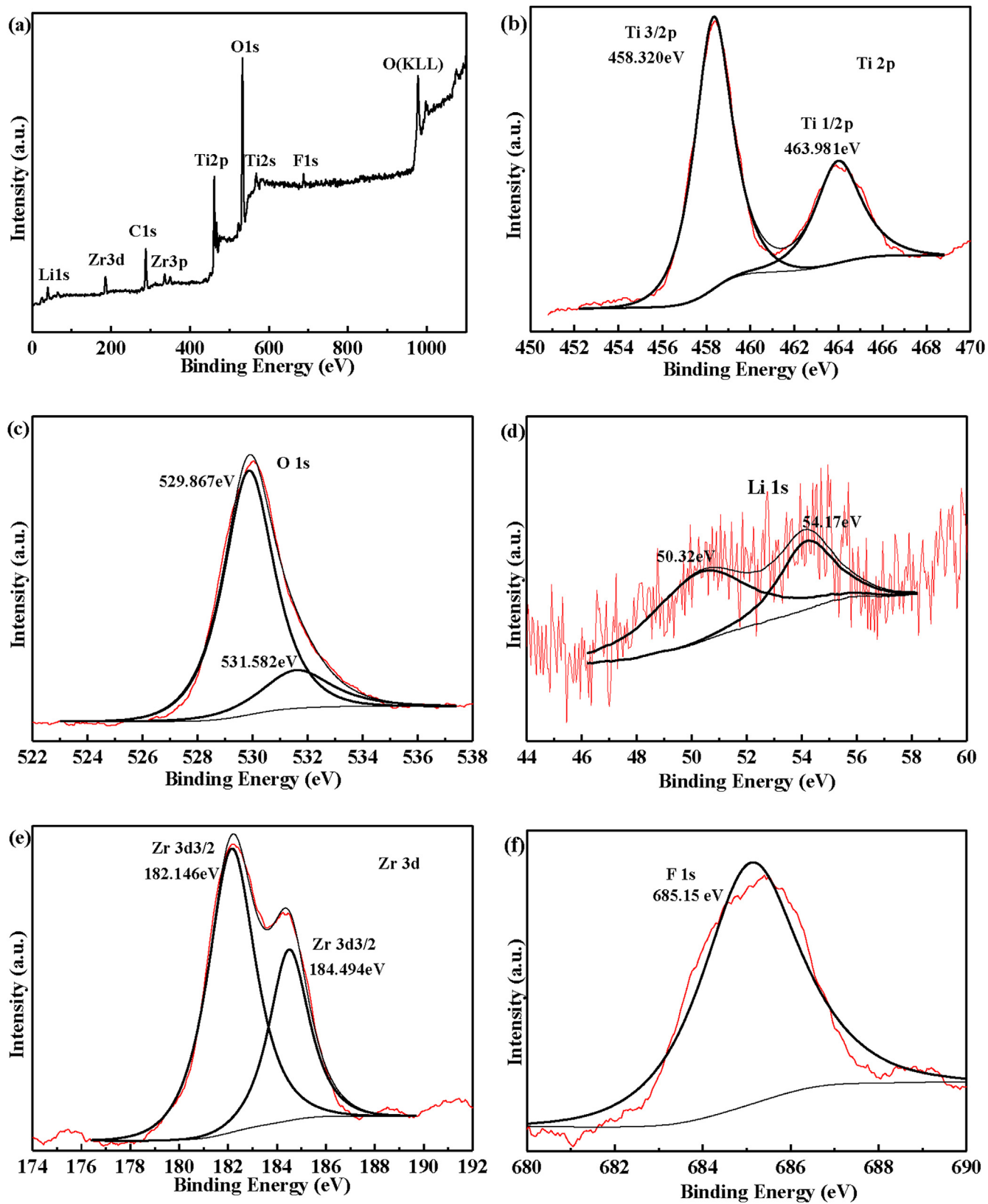


Fig. 3. (a) XPS spectrum, (b) Ti 2p, (c) O 1s, (d) Li 1s, (e) Zr 3d and (f) F 1s spectrum of 2ZrFLTO sample.

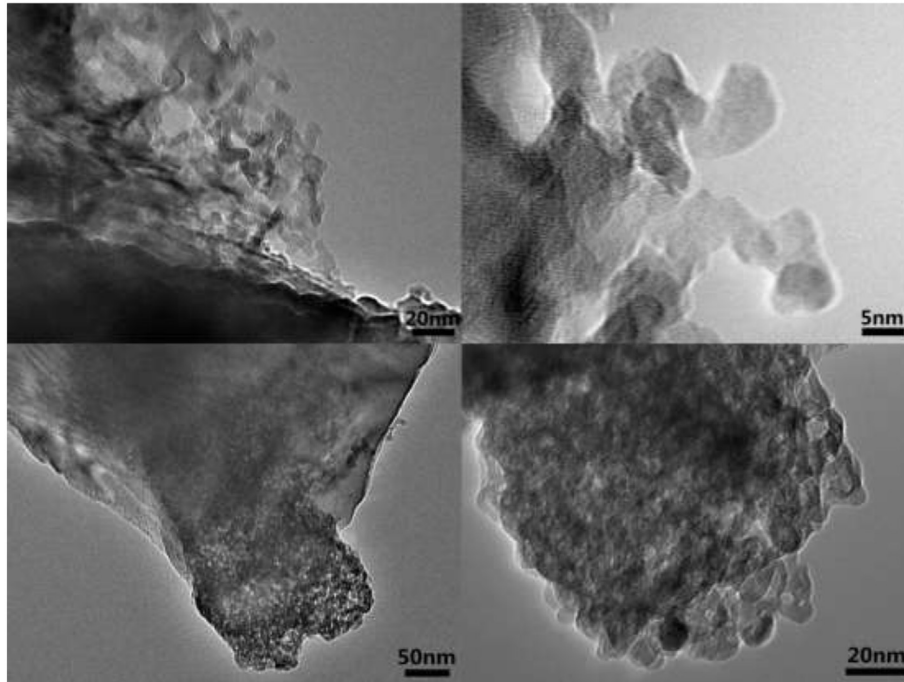


Fig. 4. HR-TEM images of (a–b) 2ZFLTO and (c–d) 2ZLTO samples.

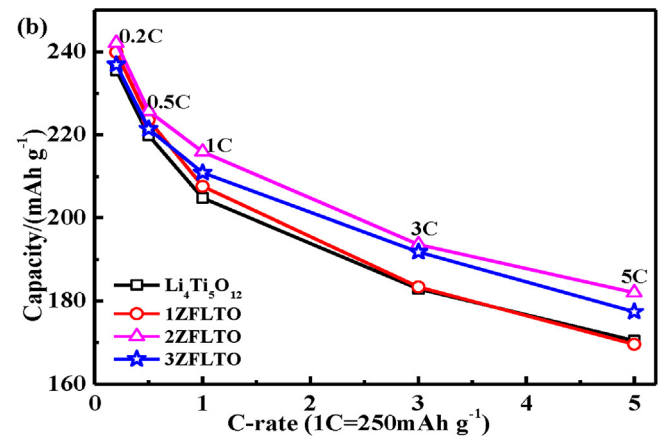
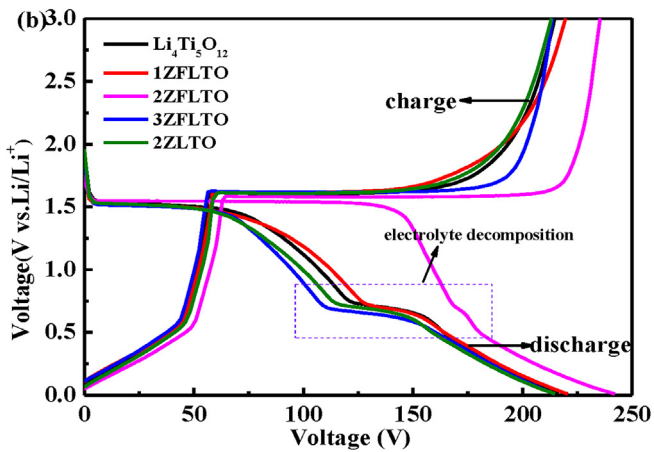
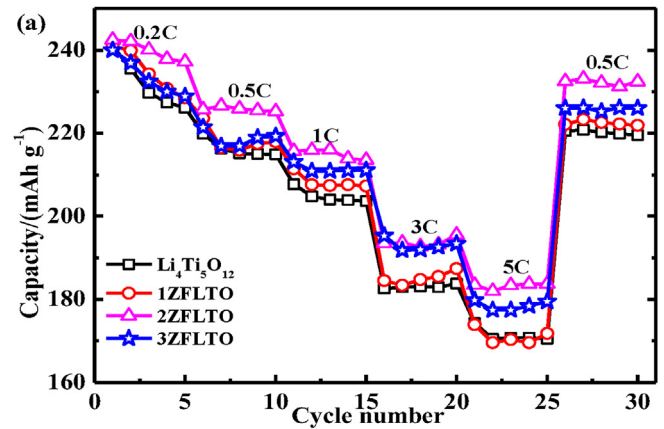
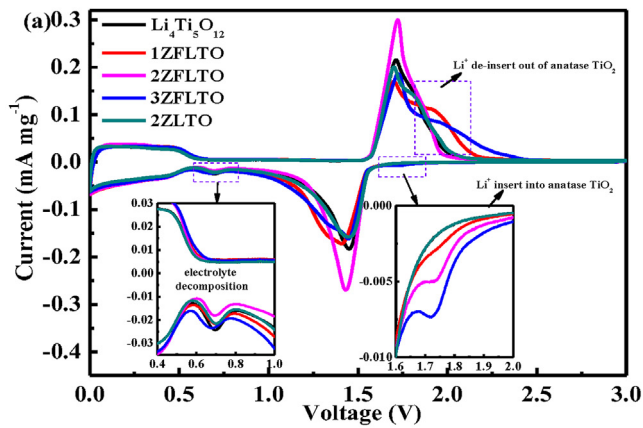


Fig. 5. (a) Cyclic voltammetry curves at a scan rate of 0.2 mV s^{-1} and (b) galvanostatic charge-discharge curves at 0.5 C -rate of the pure $\text{Li}_4\text{Ti}_5\text{O}_{12}$ and $m\text{ZFLTO}$ samples in the range of $0\text{--}3 \text{ V}$.

Fig. 6. (a) Charge capacity retention at different C-rates and (b) the second-cycle charge capacity as a function of the C-rates in the range of $0\text{--}3 \text{ V}$.

formed over the $\text{Li}_4\text{Ti}_5\text{O}_{12}$ particles.

Fig. 6a shows the charge capacity of the pure $\text{Li}_4\text{Ti}_5\text{O}_{12}$ and the *m*ZFLTO samples at various C rates in the voltage window between 0 and 3 V, and the second-cycle charge capacity at each rate is compared in Fig. 6b ($1\text{ C} = 250\text{ mAh g}^{-1}$). As it shown in Fig. 6, the 2ZFLTO and 3ZFLTO samples exhibit better rate capability than pure $\text{Li}_4\text{Ti}_5\text{O}_{12}$, suggesting that improved rate capability can be obtained by ZrF_4 -modification. It is worth mentioning that the 2ZFLTO sample delivers the best rate capability among all samples. Table 2 shows the charge capacity at different C rates of pure LTO and *m*ZFLTO samples. Pure $\text{Li}_4\text{Ti}_5\text{O}_{12}$ exhibits charge capacities of 235.5, 219.9, 204.8, 182.9 and 170.5 mAh g^{-1} at C rates of 0.2, 0.5, 1, 3, and 5, respectively. The corresponding charge capacities of 2ZFLTO are 242.1, 225.7, 215.9, 193.6 and 182.0 mAh g^{-1} , respectively, showing an improvement of 2.8%, 2.6%, 5.4%, 4.9% and 6.7% at various rates respectively. One possible reason for the improved charge capacity of 2ZFLTO is that the anatase TiO_2 formed during the modification process can act as an anode material, providing extra capacity during the lithium intercalation process. Fig. 7 shows the galvanostatic discharge-charge curves of pure $\text{Li}_4\text{Ti}_5\text{O}_{12}$ and 2ZFLTO at different C-rates in the voltage range of 0–3 V. It can be seen from Fig. 7 that there is a smaller potential difference between discharge and charge platforms of 2ZFLTO than that of pure $\text{Li}_4\text{Ti}_5\text{O}_{12}$, especially at high C rates, showing that ZrF_4 -modification is conducive to reduce the electrode polarization.

EIS was applied to investigate the electrochemical kinetics behaviors at the interface of electrolyte/electrode interface for a better understanding of rate performance. Before the discharge-charge tests, the EIS of both pure $\text{Li}_4\text{Ti}_5\text{O}_{12}$ and 2ZFLTO was performed on fresh cells. The EIS of both samples was then measured for the second time, first charging up to 1.6 V and for the third time at 21st charging up to 1.6 V, with a current density rate of 1 C in the range of 0–3 V. Next, the coin cells of both samples were first charged up to 1.6 V with a current density rate of 1 C followed by EIS measurements. Finally, after 20 cycles under the current density of 1 C, the same batteries were charged up to 1.6 V again, and EIS measurements were started. All the EIS experimental results were simulated by Z-view software using equivalent circuits inset Fig. 8a–c. The equivalent circuit (shown in Fig. 8a–c) consists of several components: the solution resistance (R_s), the resistance of the charge transfer reaction (R_{ct}), the resistance of Li^+ diffusion in the surface film layer (R_2), the resistance of electronic property change of active material (R_3), the Warburg impedance (Z_w) related to the Li^+ diffusion in solid state of active materials, the constant phase element of capacitance corresponding to R_1 (CPE1), the constant phase element of capacitance corresponding to R_2 (CPE2) and the constant phase element of capacitance corresponding to R_3 (CPE3). As illustrated, Nyquist plots of both samples at different state in the high-frequency range exhibit different features. Nyquist plots of both cells after 20 cycles and charging to 1.6 V possess three semicircles corresponding to the resistance of Li^+ diffusion in the surface film layer (HFS), resistance of the electronic property change of the active material (MFS), and resistance of the charge-transfer reaction (LFS), respectively [28] (Fig. 8c). As a

Table 2
Charge capacity at different C-rates of pure $\text{Li}_4\text{Ti}_5\text{O}_{12}$ and *m*ZFLTO samples.

Sample	Charge capacity at different C-rates (mAh g^{-1})				
	0.2 C	0.5 C	1 C	3 C	5 C
$\text{Li}_4\text{Ti}_5\text{O}_{12}$	235.5	219.9	204.8	182.9	170.5
1ZFLTO	239.9	223.6	207.6	183.4	169.6
2ZFLTO	242.1	225.7	215.9	193.6	182.0
3ZFLTO	236.9	221.4	210.9	191.8	177.4

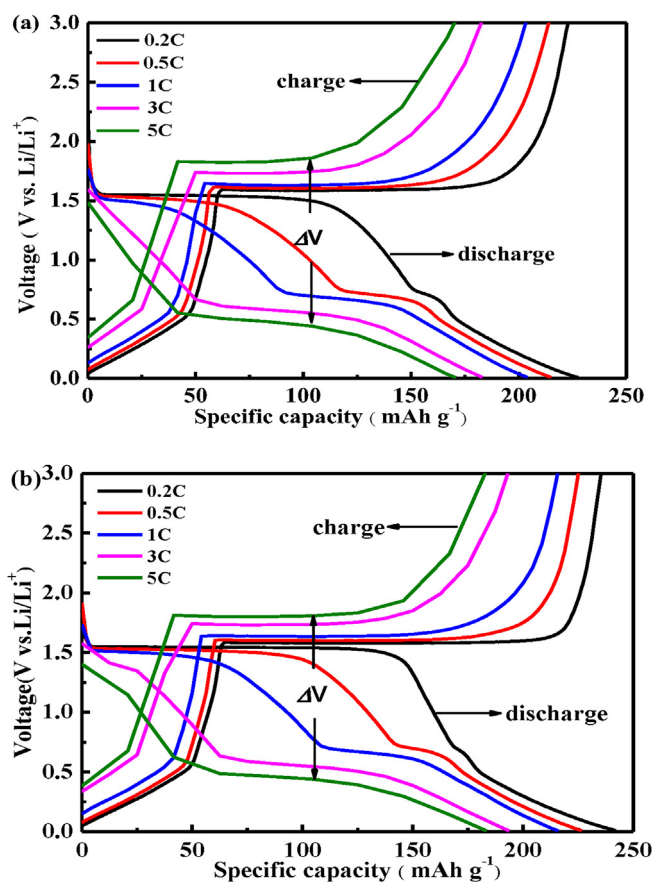


Fig. 7. Galvanostatic discharge-charge curves of (a) pure $\text{Li}_4\text{Ti}_5\text{O}_{12}$ and (b) 2ZFLTO at different C-rates in the range of 0–3 V.

comparison, Nyquist plots of cells first charged up to 1.6 V show two semicircles of HFS and LFS, and for those fresh cells only one semicircle of LFS. In the low-frequency range, a slope line is observed for those Nyquist plots of all samples, corresponding to the resistance of Li^+ diffusion in active materials (LFL). The Li^+ diffusion coefficient (D) can be calculated from the low-frequency plots according to the following equation [29,30].

$$D = \frac{R^2 T^2}{2A^2 n^4 F^4 C^2 \sigma^2} \quad (1)$$

where A is the surface area of the electrode; n the number of the electrons per molecule attending the electronic transfer reaction; F the Faraday constant; C the concentration of Li ions in the $\text{Li}_4\text{Ti}_5\text{O}_{12}$ electrode; R the gas constant; T the working temperature, which is room temperature in our experiment; and σ the slope of the line $Z \sim \omega^{-0.5}$, which can be obtained from the line of $Z \sim \omega^{-0.5}$ (shown in Fig. 8d–f) [29,30]. The impedance parameters are listed in Table 3. For the fresh cells, the absence of HFS could be due to the fact that there is almost no SEI film formed on the pure $\text{Li}_4\text{Ti}_5\text{O}_{12}$ and 2ZFLTO electrodes. The LFS value of 2ZFLTO ($108.33\ \Omega$) is higher than that of pure LTO ($60.54\ \Omega$), which could be ascribed to the fact that the impurity particles formed on the surface of 2ZFLTO are electronically uncondusive. Moreover, 2ZFLTO shows a slight higher Li^+ diffusion coefficient ($6.94 \times 10^{-14}\text{ cm}^2\text{ s}^{-1}$) than that of pure $\text{Li}_4\text{Ti}_5\text{O}_{12}$ ($3.60 \times 10^{-14}\text{ cm}^2\text{ s}^{-1}$), indicating that the modification process is likely to promote the Li^+ diffusion in the solid state of active materials. After discharge-charge cycling tests, a SEI film will be formed on the surface of the electrode material, which

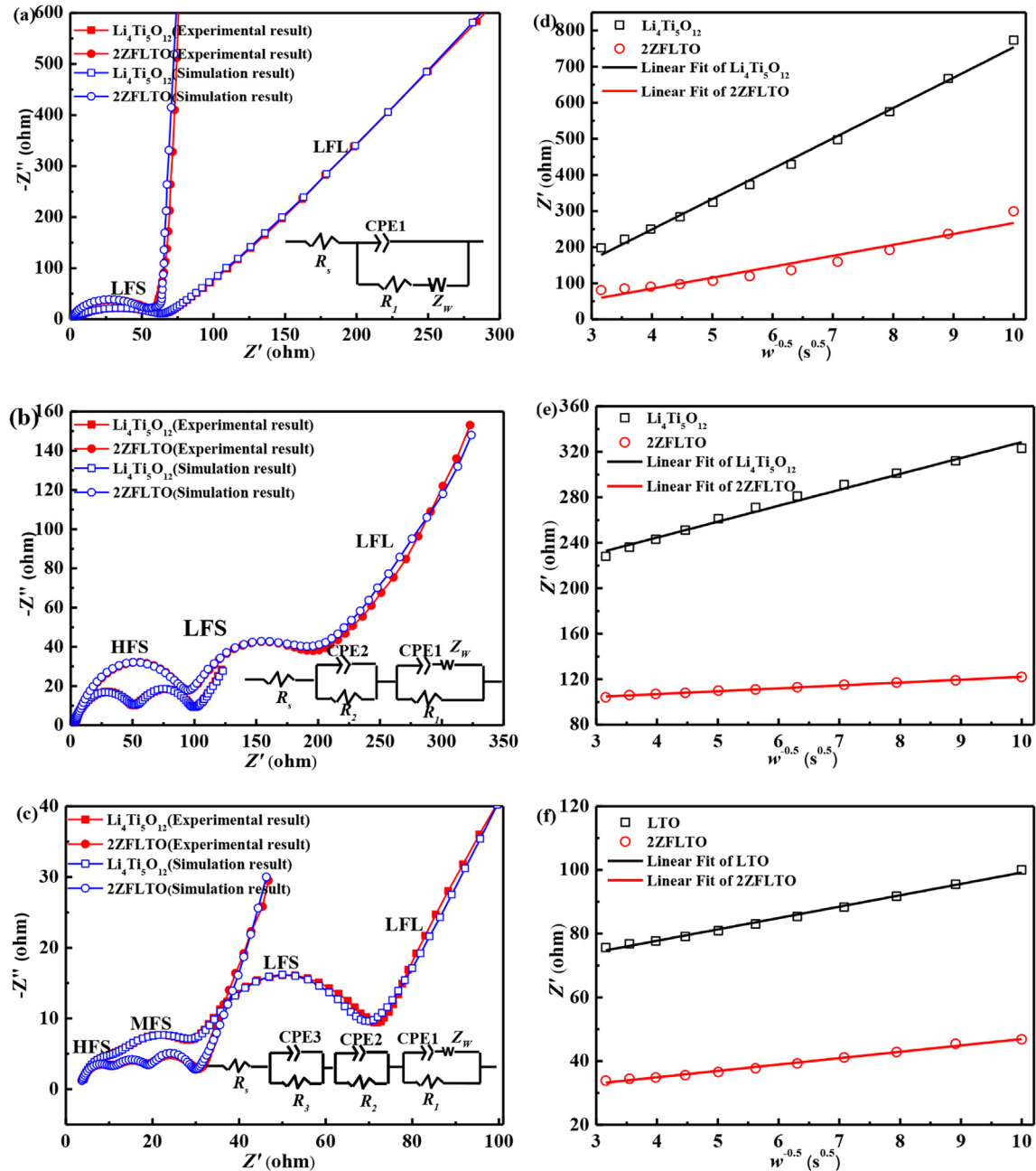


Fig. 8. (a–c) EIS curves and equivalent circuits (insert) and (d–f) $-Z''$ plotted against $\omega^{-0.5}$ at low frequency region for pure LTO and 2ZFLTO sample (a–b) Before discharge-charge cycling testing; (c–d) First charging up to 1.6 V at 1 C rate; (e–f) 21st charging up to 1.6 V at 1 C rate; HFS (resistance of Li^+ diffusion in the surface film layer); MFS (resistance of electronic property change of active material); LFS (resistance of the charge transfer reaction); LFL (resistance of Li^+ diffusion in solid state of active materials).

Table 3

The impedance parameters of EIS.

	Before cycling test		First charging up to 1.6V at 1C rate		21st charging up to 1.6V at 1C rate	
	$\text{Li}_4\text{Ti}_5\text{O}_{12}$	2ZFLTO	$\text{Li}_4\text{Ti}_5\text{O}_{12}$	2ZFLTO	$\text{Li}_4\text{Ti}_5\text{O}_{12}$	2ZFLTO
HFS (Ω)	/	/	93.92	51.54	22.23	8.73
MFS (Ω)	/	/	/	/	6.01	7.73
LFS (Ω)	60.18	54.16	94.23	42.19	33.78	9.14
σ ($\Omega \text{ cm}^2 \text{ s}^{-0.5}$)	84.04	30.24	13.98	2.54	3.57	2.00
D ($\text{cm}^2 \text{ s}^{-1}$)	3.60E-14	6.94E-14	1.30E-12	3.94E-11	1.99E-11	6.35E-11

is displayed as the semicircle of HFS in the Nyquist plots of both samples. The modification sample 2ZFLTO shows lower HFS and LFS

values than those of pure $\text{Li}_4\text{Ti}_5\text{O}_{12}$ (51.54 versus 93.92 Ω , and 42.19 versus 94.23 Ω), and show larger Li^+ diffusion coefficients than the

latter (3.94×10^{-11} versus $1.30 \times 10^{-12} \text{ cm}^2 \text{ s}^{-1}$) at first charging up to 1.6 V. 2ZFLTO delivers a lower HFS (8.73 versus 22.23 Ω), MFS (7.73 versus 6.01 Ω), and LFS (2.00 versus 3.57 Ω) values than those of pure LTO. Additionally, the Li^+ diffusion coefficient of 2ZFLTO is higher than that of pure $\text{Li}_4\text{Ti}_5\text{O}_{12}$ (6.35×10^{-11} versus $1.99 \times 10^{-11} \text{ cm}^2 \text{ s}^{-1}$) at 21st charging up to 1.6 V. The EIS results prove that both the electronic and ionic conductivity were effectively improved after modification. The surface modification can facilitate the charge-transfer reaction occurring at the interface between $\text{Li}_4\text{Ti}_5\text{O}_{12}$ particles and the electrolyte; specifically, it can promote the transport of Li^+ ions and/or electrons, as follows.

- (1) Regarding Li-ion transport, the EIS results indicate that the formed ZrO_2 nano-particles could effectively accelerate the diffusion of Li ions through SEI film, by reducing the HFS. The reason is most likely due to the fact that the formed ZrO_2 nano-particles on the surface of $\text{Li}_4\text{Ti}_5\text{O}_{12}$ particles could partly prevent the direct contact between $\text{Li}_4\text{Ti}_5\text{O}_{12}$ and the electrolyte, and cover the catalytic sites on the $\text{Li}_4\text{Ti}_5\text{O}_{12}$ surface for the decomposition of electrolyte, thereby restraining the formation of SEI film.
- (2) Regarding electron transport, it has been reported that surface modification on electrode materials can not only maintain the electron pathways between active materials and carbon additives [31,32], but also improve the adhesion of electrode materials to the current collector [31,33], thereby promoting the electron transport among them. In our case, therefore, it can be considered that ZrF_4 -modification acts in a similar way to improve electron transport and contribute to the reduced charge-transfer resistance of 2ZFLTO compared with that of pure $\text{Li}_4\text{Ti}_5\text{O}_{12}$.

Fig. 9 shows the cycling performances of pure $\text{Li}_4\text{Ti}_5\text{O}_{12}$ and mZFLTO samples at a 5-C rate, and the corresponding results are listed in Table 4. After 100 cycles, the charge capacity retention of pure $\text{Li}_4\text{Ti}_5\text{O}_{12}$ is 93.8%, while that of the 2ZFLTO samples is 98.5%. The modification sample shows slight higher capacity retention than the pure sample, suggesting that 2-wt% ZrF_4 -modification can improve the cycling performance of $\text{Li}_4\text{Ti}_5\text{O}_{12}$. This illustrates that the Zr^{4+} and F^- co-modification process benefits enhancement the cycling stability at a high C rate, due to the fact that the formation of both ZrO_2 nano-particles and LiF over the 2ZFLTO particles are beneficial to preventing the electrolyte reduction decomposition, and to suppressing the gas generation, which is conducive to the

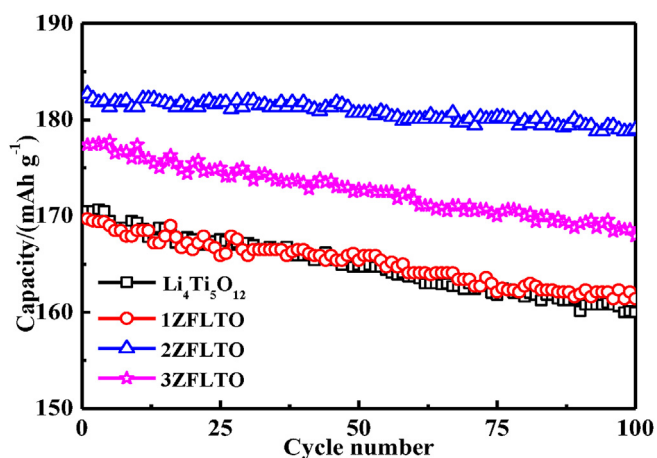


Fig. 9. Cycling stability of pure $\text{Li}_4\text{Ti}_5\text{O}_{12}$ and mZFLTO samples at 5 C rate in the range of 0–3 V.

Table 4

The charge capacity retention pure $\text{Li}_4\text{Ti}_5\text{O}_{12}$ and mZFLTO samples at 5 C rate.

Sample	Charge capacity in the range of 0–3 V (mA h g^{-1})		Capacity retention (%)
	1 st cycle	100 th cycle	
$\text{Li}_4\text{Ti}_5\text{O}_{12}$	170.5	160.0	93.8
1ZFLTO	169.7	161.4	95.1
2ZFLTO	182.7	179.0	98.5
3ZFLTO	177.4	167.9	94.6

cycling performance of $\text{Li}_4\text{Ti}_5\text{O}_{12}$.

4. Conclusions

The reaction mechanism of the ZrF_4 -modification process was different from other such processes, e.g., AlF_3 , MgF_2 , ZnF_2 , SrF_2 , and CaF_2 modification which had been previously reported [17–22]. After the ZrF_4 -modification process, F^- reacts with $\text{Li}_4\text{Ti}_5\text{O}_{12}$ chemically to generate a new impurity phase, such as anatase TiO_2 and LiF, while Zr^{4+} forms amorphous ZrO_2 nano-particles over the $\text{Li}_4\text{Ti}_5\text{O}_{12}$ particles. The nano-particles cannot cover all the $\text{Li}_4\text{Ti}_5\text{O}_{12}$ particles, with the nano-particles layer over the $\text{Li}_4\text{Ti}_5\text{O}_{12}$ particles being non-continuous. Because no dense ZrO_2 coating layer was formed on the surface of the $\text{Li}_4\text{Ti}_5\text{O}_{12}$ particles, the catalytic sites on the $\text{Li}_4\text{Ti}_5\text{O}_{12}$ surface for the decomposition of electrolyte could not be covered completely. However, the new phase formed over the $\text{Li}_4\text{Ti}_5\text{O}_{12}$ particles could partly suppress the decomposition of electrolyte, thereby restraining SEI formation, promoting electron transport across the electrode/electrolyte interface and thus reducing the charge-transfer resistance. Meanwhile, ZrF_4 -modification is conducive to reducing the electrode polarization. Therefore, the rate capability of $\text{Li}_4\text{Ti}_5\text{O}_{12}$ electrode materials can be improved by ZrF_4 modification. In addition, the formation of both ZrO_2 nano-particles and LiF over the $\text{Li}_4\text{Ti}_5\text{O}_{12}$ particles is beneficial to preventing the electrolyte reduction decomposition, and to suppressing the gas generation, which is conducive to the cycling performance of $\text{Li}_4\text{Ti}_5\text{O}_{12}$. The 2ZFLTO sample, in particular, it delivers the best electrochemical performances among all the modified samples.

Acknowledgments

This work was carried out with financial support from Hebei Province Applied Basic Research Program-Key Basic Research Project (17964407D), Science and Technology Program of Hebei Province (17394411D), Project of Hebei Academy of Science (171407) and Project of Hebei Academy of Science (171413).

References

- [1] Y.K. Sun, J.M. Han, S.T. Myung, S.W. Lee, K. Amine, Significant improvement of high voltage cycling behavior AlF_3 -coated LiCoO_2 cathode, *Electrochem. Commun.* 8 (2006) 821–826.
- [2] Y.K. Sun, S.W. Cho, S.T. Myung, K. Amine, J. Prakash, Effect of AlF_3 coating amount on high voltage cycling performance of LiCoO_2 , *Electrochim. Acta* 53 (2007) 1013–1019.
- [3] K.S. Lee, S.T. Myung, D.W. Kim, Y.K. Sun, AlF_3 -coated LiCoO_2 and $\text{Li}[\text{Ni}_{1/3}\text{Co}_{1/3}\text{Mn}_{1/3}]\text{O}_2$ blend composite cathode for lithium ion batteries, *J. Power Sources* 196 (2011) 6974–6977.
- [4] G.M. Song, Y. Wu, G. Liu, Q. Xu, Influence of AlF_3 coating on the electrochemical properties of $\text{LiFePO}_4/\text{graphite}$ Li-ion batteries, *J. Alloys Compd.* 487 (2009) 214–217.
- [5] B.C. Park, H.B. Kim, S.T. Myung, K. Amine, I. Belharouak, S.M. Lee, Y.K. Sun, Improvement of structural and electrochemical properties of AlF_3 -coated $\text{Li}[\text{Ni}_{1/3}\text{Co}_{1/3}\text{Mn}_{1/3}]\text{O}_2$ cathode materials on high voltage region, *J. Power Sources* 178 (2008) 826–831.
- [6] S.H. Lee, C.S. Yoon, K. Amine, Y.K. Sun, Improvement of long-term cycling performance of $\text{Li}[\text{Ni}_{0.8}\text{Co}_{0.15}\text{Al}_{0.05}]\text{O}_2$ by AlF_3 coating, *J. Power Sources* 234

- (2013) 201–207.
- [7] Y.K. Sun, M.J. Lee, C.S. Yoon, J. Hassoun, K. Amine, B. Scrosati, The role of AlF_3 coatings in improving electrochemical cycling of Li-enriched nickel-manganese oxide electrodes for Li-ion batteries, *Adv. Mater.* 24 (2012) 1192–1196.
- [8] J.M. Zheng, M. Gu, J. Xiao, B.J. Polzin, P.F. Yan, X.L. Chen, C.M. Wang, J.G. Zhang, Functioning mechanism of AlF_3 coating on the Li- and Mn-rich cathode materials, *Chem. Mater.* 26 (2014) 6320–6327.
- [9] F. Ding, W. Xu, D.W. Choi, W. Wang, X.L. Li, M.H. Engelhard, X.L. Chen, Z.G. Yang, J.G. Zhang, Enhanced performance of graphite anode materials by AlF_3 coating for lithium-ion batteries, *J. Mater. Chem.* 22 (2012) 12745–12751.
- [10] J.G. Li, X.M. He, R.S. Zhao, Electrochemical performance of SrF_2 -coated LiMn_2O_4 cathode material for Li-ion batteries, *Trans. Nonferrous Met. Soc. China* 17 (2007) 1324–1327.
- [11] J.G. Li, L. Wang, Q. Zhang, X.M. He, Electrochemical performance of SrF_2 -coated $\text{LiNi}_{1/3}\text{Co}_{1/3}\text{Mn}_{1/3}\text{O}_2$ cathode materials for Li-ion batteries, *J. Power Sources* 190 (2009) 149–153.
- [12] K. Xu, Z.F. Jie, R.H. Li, Z.X. Chen, S.T. Wu, J.F. Gu, J.Z. Chen, Synthesis and electrochemical properties of CaF_2 -coated for long-cycling $\text{Li}[\text{Mn}_{1/3}\text{Co}_{1/3}\text{Ni}_{1/3}]\text{O}_2$ cathode materials, *Electrochim. Acta* 60 (2012) 130–133.
- [13] S.J. Shi, J.P. Tu, Y.J. Mai, Y.Q. Zhang, Y.Y. Tang, X.L. Wang, Structure and electrochemical performance of CaF_2 coated $\text{LiMn}_{1/3}\text{Ni}_{1/3}\text{Co}_{1/3}\text{O}_2$ cathode material for Li-ion batteries, *Electrochim. Acta* 83 (2012) 105–112.
- [14] S.J. Shi, J.P. Tu, Y.Y. Tang, Y.Q. Zhang, X.Y. Liu, X.L. Wang, C.D. Gu, Enhanced electrochemical performance of LiF-modified $\text{LiNi}_{1/3}\text{Co}_{1/3}\text{Mn}_{1/3}\text{O}_2$ cathode materials for Li-ion batteries, *J. Power Sources* 225 (2013) 338–346.
- [15] S.H. Yun, K.S. Park, Y.J. Park, The electrochemical property of ZrF_x -coated $\text{Li}[\text{Ni}_{1/3}\text{Co}_{1/3}\text{Mn}_{1/3}]\text{O}_2$ cathode material, *J. Power Sources* 195 (2010) 6108–6115.
- [16] Z.X. Yang, Q.D. Qiao, W.S. Yang, Improvement of structural and electrochemical properties of commercial LiCoO_2 by coating with LaF_3 , *Electrochim. Acta* 56 (2011) 4791–4796.
- [17] W. Xu, X.L. Chen, W. Wang, D.W. Choi, F. Ding, J.M. Zheng, Z.M. Nie, Y.J. Choi, J.G. Zhang, Z.G. Yang, Simply AlF_3 -treated $\text{Li}_4\text{Ti}_5\text{O}_{12}$ composite anode materials for stable and ultrahigh power lithium-ion batteries, *J. Power Sources* 236 (2013) 169–174.
- [18] W. Li, X. Li, M.Z. Chen, Z.W. Xie, J.X. Zhang, S.Q. Dong, M.Z. Qu, AlF_3 modification to suppress the gas generation of $\text{Li}_4\text{Ti}_5\text{O}_{12}$ anode battery, *Electrochim. Acta* 139 (2014) 104–110.
- [19] W. Li, H. Wang, M.Z. Chen, J.J. Gao, X. Li, W.J. Ge, M.Z. Qu, A.J. Wei, L.H. Zhang, Z.F. Liu, The reaction mechanism of the Mg^{2+} and F^- co-modification and its influence on the electrochemical performance of the $\text{Li}_4\text{Ti}_5\text{O}_{12}$ anode material, *Electrochim. Acta* 188 (2016) 499–511.
- [20] A.J. Wei, W. Li, L.H. Zhang, X.H. Li, X. Bai, Z.F. Liu, Effect of Zn^{2+} and F^- co-modification on the structure and electrochemical performance of $\text{Li}_4\text{Ti}_5\text{O}_{12}$ anode material, *Nano* 12 (2017) 17500541–17500549.
- [21] X. Li, X. Zhao, P.X. Huang, M.S. Wang, Y. Huang, Y. Zhou, Y.H. Lin, M.Z. Qu, Z.L. Yu, Enhanced electrochemical performance of SrF_2 -modified $\text{Li}_4\text{Ti}_5\text{O}_{12}$ composite anode materials for lithium-ion batteries, *J. Alloys Compd.* 693 (2017) 61–69.
- [22] W. Li, A.J. Wei, L.H. Zhang, X.H. Li, X. Bai, Z.F. Liu, Structure and enhanced electrochemical performance of the CaF_2 -modified $\text{Li}_4\text{Ti}_5\text{O}_{12}$ anode material, *J. Electroanal. Chem.* 791 (2017) 196–203.
- [23] J.G. Kim, M.S. Park, S.M. Hwang, Y.U. Heo, T. Liao, Z. Sun, J.H. Park, K.J. Kim, G. Jeong, Y.J. Kim, J.H. Kim, S. Dou, Zr^{4+} Doping in $\text{Li}_4\text{Ti}_5\text{O}_{12}$ anode for lithium-ion batteries: open Li^+ diffusion paths through structural imperfection, *ChemSusChem* 7 (2014) 1451–1457.
- [24] X. Li, M.Z. Qu, Z.L. Yu, Structural and electrochemical performances of $\text{Li}_4\text{Ti}_{5-x}\text{Zr}_x\text{O}_{12}$ as anode material for lithium-ion batteries, *J. Alloys Compd.* 487 (2009) L12–L17.
- [25] R.D. Shannon, Revised effective ionic radii and systematic studies of interatomic distances in halides and chalcogenides, *Acta Crystallogr.* 32 (1976) 751–767.
- [26] Y. Ma, B. Ding, G. Ji, J.Y. Lee, Carbon-encapsulated F-Doped $\text{Li}_4\text{Ti}_5\text{O}_{12}$ as a high rate anode material for Li^+ batteries, *ACS Nano* 7 (2013) 10870–10878.
- [27] X. Bai, W. Li, A.J. Wei, X.H. Li, L.H. Zhang, Z.F. Liu, Preparation and electrochemical properties of Mg^{2+} and F^- co-doped $\text{Li}_4\text{Ti}_5\text{O}_{12}$ anode material for use in the lithium-ion batteries, *Electrochim. Acta* 222 (2016) 1045–1055.
- [28] J. Chong, J.P. Zhang, H.M. Xie, X.Y. Song, G. Liu, V. Battaglia, S.D. Xun, R.S. Wang, High performance $\text{LiNi}_{0.5}\text{Mn}_{1.5}\text{O}_4$ cathode material with a bi-functional coating for lithium ion batteries, *RSC Adv.* 6 (2016) 19245–19251.
- [29] H.P. Liu, G.W. Wen, S.F. Bi, P. Gao, Enhanced rate performance of nanosized $\text{Li}_4\text{Ti}_5\text{O}_{12}$ /graphene composites as anode material by a solid state-assembly method, *Electrochim. Acta* 171 (2015) 114–120.
- [30] Q.Y. Zhang, M.G. Verde, J.K. Seo, X. Li, Y.S. Meng, Structural and electrochemical properties of Gd-doped $\text{Li}_4\text{Ti}_5\text{O}_{12}$ as anode material with improved rate capability for lithium-ion batteries, *J. Power Sources* 280 (2015) 355–362.
- [31] J. Liu, X.F. Li, M. Cai, R.Y. Li, X.L. Sun, Ultrathin atomic layer deposited ZrO_2 coating to enhance the electrochemical performance of $\text{Li}_4\text{Ti}_5\text{O}_{12}$ as an anode material, *Electrochim. Acta* 93 (2013) 195–201.
- [32] Y.S. Jung, A.S. Cavanagh, L.A. Riley, S.H. Kang, A.C. Dillon, M.D. Groner, S.M. George, S.H. Lee, Ultrathin direct atomic layer deposition on composite electrodes for highly durable and safe Li-ion batteries, *Adv. Mater.* 22 (2010) 2172–2176.
- [33] L.A. Riley, A.S. Cavanagh, S.M. George, S.H. Lee, A.C. Dillon, Improved mechanical integrity of ALD-coated composite electrodes for Li-ion batteries, *Electrochem. Solid State Lett.* 14 (2011) A29–A31.